Journal of Materials Chemistry A

Accepted Manuscript

ROYAL SOCIETY OF CHEMISTRY

www.rsc.org/materialsA

Journal of Materials Chemistry A

Graphical Abstract

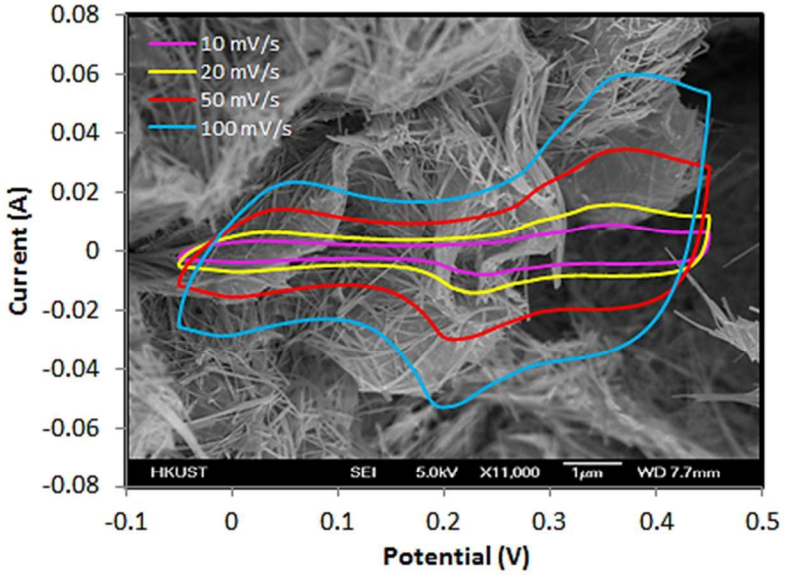

Materials Chemistry A

ARTICLE

Controlled synthesis of cobalt carbonate/graphene composites with excellent supercapacitive performance and pseudocapacitive characteristics

Cite this: DOI: 10.1039/x0xx00000x

Mohammad Akbari Garakani[a], Sara Abouali[a], Biao Zhang[a], Zheng-Long Xu[a], Jiaqiang Huang[a], Jian-Qiu Huang[a], Elham Kamali Heidari[a], Jang-Kyo Kim[a] *

Received 00th June 2012,
Accepted 00th June 2012

DOI: 10.1039/x0xx00000x

www.rsc.org/

Cobalt carbonate hydroxide/graphene aerogel and cobalt carbonate/graphene aerogel (CCH/GA and CC/GA) composites are synthesized as supercapacitor electrodes via a one-pot hydrothermal method. Optimized processing conditions are established by controlling the composite composition and microstructure, and their influences on capacitance performance of the electrodes are identified. A remarkable specific capacitance of 1134 F g^{-1} at a current density of 1 A g^{-1} is obtained for the optimal nanowire-shaped CCH/GA electrode, which is among the highest capacitance of cobalt compound electrodes with or without nanocarbons reported so far. The electrode also delivers exceptional rate performance and cyclic stability benefiting from the pseudocapacitive characteristics of CC-based active material and the highly conductive, interconnected 3D-structured GA. The CC/GA electrode presents a high capacity of 731 F g^{-1} under the same condition. The *ex situ* XPS analysis identifies the reversible redox reactions of cobalt cations during charge/discharge cycles as the electrochemical mechanism responsible for the high pseudocapacitive properties of CC-based electrodes.

1. Introduction

Supercapacitors (SCs) are considered a promising candidate for energy storage devices owing to their higher power densities and longer cyclic life than rechargeable batteries and higher energy densities than conventional dielectric capacitors. In addition, SCs are capable of storing and delivering energies at relatively high rates.[1-3] Considerable efforts are still ongoing to identify ideal electrode materials for SCs which possess both high capacitances and excellent cyclic stability.

Based on the electrode charge storage mechanisms, SCs can be divided into two types. The first is the electric double-layer capacitors (EDLCs) where energy is stored by charge separation at the electrochemical interface between the electrode and the electrolyte. In EDLCs, the surface storage mechanism allows very fast energy uptake and delivery, and thus high power performance.[1,4] Highly conductive carbon materials with large surface areas have been widely used as the electrode material for EDLCs. Among many carbon materials, graphene is known to be an ideal candidate for SC applications, due to its large theoretical surface area and high electrical conductivity.[5,6] The second is pseudocapacitors (PCs) that utilize pseudo Faradaic reactions in addition to double layers for charge storage. In PCs, the stability during the charge/discharge cycles is relatively poor although their energy densities are higher than EDLCs. The response time in PCs is longer than EDLCs because it takes long to move electrons during the redox reactions.[7,8] PC materials, such as transition metal oxides[9,10] and hydroxides,[11,12] possess high capacitances originating from the redox reactions. Metal hydroxides usually show higher specific capacitances than oxides because the high temperature calcination process to convert hydroxides to oxides may result in the elimination of surface defects and the decrease in hydrate content, leading to performance degradation.[13] Other transition metal compounds, such as nitrates, carbonates and hydroxy oxides, have also been explored as solid precursors to synthesize their respective nanostructured metal-oxides through one or more chemical/thermal conversion process(es). Among them, metal carbonates are abundant and widely used in industry, thus the synthesis of these compounds is extensively studied in recent years.[14] Nevertheless, very few studies have so far been reported on their applications in energy storage devices, and their potentials as the PC electrodes are uncertain.[15,16]

PCs often suffer from low rate capability and poor cyclic stability because the poor electrical conductivities of the electrodes hinder electron transport required for high charge/discharge rates.[17,18] Several strategies have been proposed to address this issue. Among them, fabricating nanocomposites consisting of a carbon material(s) and a

transition metal oxide has attracted much attention due to their synergistic effects arising from the combination of redox reactions of metal oxides, and high electrical conductivity and large surface area of carbon materials.[19] Different types of carbon, such as carbon nanotubes,[20] carbon nanofibers,[21] activated carbon[22] and graphene,[23,24] have been employed as the matrix or support to prepare nanocomposite electrodes. However, most of the reported synthesis methods require multi-step processes involving carbonization and/or transformation of transition metal compounds to oxides. This not only makes the synthesis complicated with limited potentials for large-scale applications, but also makes it difficult to find an optimized heat treatment condition.[25-27] Therefore, designing a facile strategy to synthesize high capacity composite electrodes has been a great challenge.

With the aforementioned issues in mind, we made a systematic study to optimize the processing conditions and compositions for the synthesis of composites containing cobalt carbonate hydroxide nanowire/graphene aerogel or cobalt carbonate microcube/graphene aerogel (CCH/GA and CC/GA). The influences of urea as the source of carbonate anions on the evolution of active materials from CCH to CC, as well as the synergetic effect of hybridizing graphene aerogels are specifically investigated. The pseudocapacitive mechanisms of the CC-based electrodes are established and the reversible redox reactions responsible for excellent specific capacitances are proposed.

2. Experimental section

2.1. Synthesis of active materials

GO dispersion was prepared based on the modified Hummers method as in the previous studies.[28,29] Briefly, graphite flakes were thermally expanded at 1050 ˚C for 15 s after intercalation with H_2SO_4 and HNO_3 to obtain expanded graphite (EG). H_2SO_4 and $KMnO_4$ were mixed with EG and kept at 60 ˚C for 24 h. The mixture was transferred to an ice bath, deionized (DI) water and later, H_2O_2 was added. After stirring for 30 min, the GO particles were washed with HCl solution and centrifuged three times. DI water was used to wash the GO until the pH reached 5–6. The GO solution was further diluted with DI water to a desirable concentration. To identify the optimized compositions and processing conditions, different mass ratios of $CoCl_2$. $6H_2O$ as the cobalt precursor and urea as the source of carbonate anions were added to the GO dispersion of different concentrations and stirred for 1 h (Table 1). The mixture was transferred to a 45 ml Teflon-lined stainless steel autoclave, and treated at 180 ˚C for 12 h. After cooling to room temperature, the graphene hydrogel containing cobalt carbonate-based particles with light-pink deposits was washed with DI water. The products were stored at -20 ˚C for 24 h and then freeze-dried at -60 ˚C for 24 h in a freeze drier (Edwards Pirani 501 Super Modulyo Freeze Drier, Thermo Electron Corporation) to obtain CCH/GA or CC/GA composites. Table 1 shows the compositions and the corresponding designations of the composites. To have a better comparison, neat active materials without graphene were also prepared using the same processing conditions (CCH/GA-0).

Table 1. Compositions and corresponding designations of different electrode materials.

Designations	Compositions GO:$CoCl_2$:Urea (mg:mmol:mmol)/30 mL DI water	Electrical Conductivity (S cm^{-1})	BET Surface Area (m^2 g^{-1})
CCH/GA-0	0:1:1	1.2×10^{-5}	16.5
CCH/GA-1	60:3:3	1.3×10^{-1}	32.5
CCH/GA-2	30:3:3	1.5×10^{-2}	31.4
CCH/GA-3	30:4.5:3	2.8×10^{-3}	22.9
CC/GA-1	30:3:15	3.5×10^{-2}	8.7
CC/GA-2	30:3:30	2.5×10^{-2}	5.5
CC/GA-3	30:3:60	4.6×10^{-2}	7.2

2.2. Characterization

The microstructures of composites were characterized on a powder X-ray diffraction (XRD) system (PW1830, Philips) with Cu K α radiation from 20˚ to 80˚. Scanning electron microscopy (SEM, JEOL 6300) and field emission transmission electron microscopy (FETEM, JEOL 2010F) were used to examine the micro and nanostructural features and morphologies. The surface area was measured using the Brunauer–Emmett–Teller (BET) method on a Coulter SA 3100 Surface Area instrument. The electrical conductivities were determined using the pressed pallets of materials on a four-probe resistivity/Hall system (HL5500PC, Bio-Rad). Thermogravimetric analysis (TGA) was conducted (TGA/DTA 92 Setaram II testing system) in air over a temperature range of 50–800°C at a heating rate of 10 °C min^{-1}. The X–ray photoelectron spectroscopy (XPS, Surface analysis PHI5600, Physical Electronics) was employed to evaluate the surface elemental compositions of the materials, using Al K α line as the excitation source.

2.3. Electrochemical measurements

The working electrode was prepared by mixing the composites with conductive carbon black (super P) and polyvinylidene fluoride (PVDF) as the binder dissolved in N-methyl-2-pyrrolidone (NMP) in the weight ratio of 70:10:20. The resulting mixture was coated onto the 10 mm x 10 mm Ni foam substrate with electrode mass loading of ~0.8 mg/cm^2 and dried at 80 ˚C for 12 h in air before using as the current collector. The electrochemical performance of the electrodes was measured using a three-electrode cell in 6 M KOH aqueous electrolyte at room temperature. A platinum mesh and a saturated Ag/AgCl electrode were used as the counter and reference electrodes, respectively. Cyclic voltammetry (CV) and galvanostatic charge/discharge (GCD) tests were performed on an electrochemical workstation (CHI 660C) at potentials ranging between -0.05 and 0.45 V at different scanning rates from 10 to 100 mV s^{-1} and current densities from 1 to 10 A g^{-1}. The specific capacitance (C_s) was calculated using the GCD data according to the equation:

$$C_s = \frac{It}{m\Delta V} \quad (1)$$

where I is the applied current, t is the time for discharge process, m is the mass of the active material and ΔV is the potential range. Electrochemical impedance spectroscopy (EIS) was carried out in the range of frequency 100 kHz–0.01 Hz at an

open circuit potential. In order to have a better evaluation of the electrochemical performance, cells made from the optimized material were assembled in a two-electrode configuration using two pieces of identical electrodes separated by a filter paper as the separator, and the assembly was soaked in 6 M KOH for 12 h. The measurements were carried out at the same potential range, and the gravimetric specific capacitance, Cs (F g^{-1}), for the whole cell was calculated from the GCD curve according to Equation (1) and considering the total mass of the two electrodes.[30,31]

3. Results and Discussion

Fig. 1 shows the XRD patterns of different electrode materials. The major peaks in the composites, CCH/GA-x where x = 0-3, containing a small amount (i.e. 3 mmol or below) of urea were located at 26.7, 28.7, 30.4, 33.8, 35.4, 36.5, 39.5, 44.6, 47.3, 54.0, 56.06, 59.8 and 62.2 degrees corresponding to the (220), (121), (300), (221), (040), (301), (231), (050), (340), (060), (142), (412) and (450) reflections, respectively, signifying the presence of cobalt carbonate hydroxide hydrate (CCH) (JCPDS no. 00-048-0083). Most of the peaks of the composites, CC/GA-x, containing a large amount (i.e. above 3 mmol) of urea were located at 25.0, 32.6, 38.5, 42.7, 46.5, 51.3, 53.9, 62.0, 66.0 and 68.3 degrees corresponding to the (012), (104), (110), (113), (202), (024), (018), (122), (214) and (208) reflections, respectively, showing cobalt carbonate (CC) (JCPDS no. 01-078-0209). These results indicate that it is more likely to form CC than CCH during the hydrothermal process with increasing urea content.

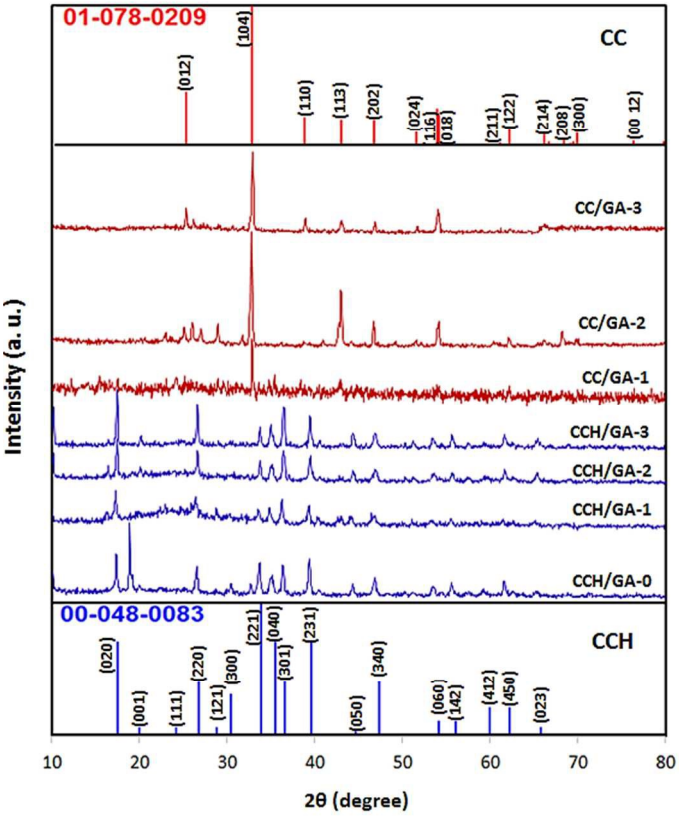

Fig. 1 XRD patterns indicating the transformation of CCH to CC with increasing urea content.

CC-based compounds were synthesized by a facile hydrothermal process according to the below reactions. Urea, $CO(NH_2)_2$, possibly contains both physisorbed and chemisorbed water, especially when it is formed in an aqueous solution. Here, it acted as the source of both carbonate and hydroxyl anions (Equations 3 and 4) by decomposition in water during the hydrothermal process, while the cobalt cations came from cobalt chloride. Therefore, CC was produced according to Equation 5, whereas CCH was produced according to Equation 6.[27,32]

$$CO(NH_2)_2 + 3H_2O \rightarrow 2NH_4^+ + CO_2 + 2OH^- \quad (3)$$

$$CO_2 + 2OH^- \rightarrow CO_3^{2-} + H_2O \quad (4)$$

$$Co^{2+} + CO_3^{2-} \rightarrow CoCO_3 \quad (5)$$

$$Co^{2+} + 0.5CO_3^{2-} + OH^- + 0.11H_2O \rightarrow Co(CO_3)_{0.5}(OH).0.11H_2O \quad (6)$$

These reactions also indicate that more carbonate anions were released when the urea content was increased, more likely to form CC than CCH, in agreement with the XRD results.

Fig. 2a shows the TEM images of CCH without graphene (CCH/GA-0) in the form of nanowires. The selected area electron diffraction (SAED) pattern in the inset of Fig. 2a presents the diffractions of the (020) and (300) planes in the CCH single crystal. The HRTEM image along with the corresponding fast Fourier transform (FFT) pattern (Fig. 2b and inset) show these two planes with d-spacing of 0.506 and 0.293 nm, respectively. The direction of crystal growth was also indicated along [100] in Figs. 2a and b. The elemental mapping images and energy-dispersive X-ray spectroscopy (EDS) results in Figs. 2c and d confirmed the existence of Co, O and C atoms. All these findings are in agreement with the XRD result and the aforementioned reactions, substantiating the formation of CCH single crystals during the hydrothermal process.

The composite samples were synthesized under the same hydrothermal conditions and Fig. 3 presents typical SEM and TEM images of CCH/GA-2 composite (which had the best electrochemical performance among all composite electrodes prepared in this study to be discussed later). The CCH nanowires were uniformly dispersed between the graphene sheets of the 3D GA structure (Fig. 3a and b). The effect of urea content on morphology and size of the CC-based particles were specifically studied, and the matching SEM images are shown in Fig. S1. It is revealed that the increase in urea content resulted in not only the change in atomic structure of the active materials (Fig. 1), but also the unique transition of their morphologies from 1D nanowires (CCH/GA-2) to a mixture of 1D CCH nanowires and 3D CC sub-micro cubes (CC/GA-1, Fig. S1a), and finally to 3D CC microcubes with few tens of micrometer in diameter (CC/GA-3, Fig. S1b). The change in morphology into a more compact structure and the larger active particle size led to much reduced surface areas (Table 1), with potentially weaker interfacial contacts and possible detachment of the active materials from the graphene matrix (Fig. S1b). As a consequence, the electrochemical performance of the CC/GA electrodes was adversely influenced by these changes, which will be discussed in the following. Because the formation of carbonate depends largely on the dissolution of CO_2 gas (Equation 4), CC became more difficult to form when the amount of urea supply in the synthesis was on the lower side (Equation 5).[33] From materials chemistry point of view, the carbonate anions also acted as inhibitors which selectively discouraged the crystal growth of a nanowire structure,[13] resulting in a distinct morphological evolution from CCH nanowire to sub-microcubes and microcubes of CC. The formation of these CC sub-micrometer crystals can be

explained by a sequential mechanism of precipitation-dissolution-renucleation-growth-aggregation where, at the initial stage, the primary precipitates were formed when supersaturation in the solution was reached. The process was followed by dissolution of unstable precipitates which was then turned into renucleation and growth of crystallites. The resultant crystallites were aggregated and/or attached onto the final crystals to minimize the interfacial energy.[33,34] These observations signify that urea played an important role not only in providing the hydroxyl and carbonate groups, but also in controlling the final composition and morphology of the active materials. Similar investigations of shape control by changing the urea content have been reported for other transition metal compounds, such as NiO,[35] Co_3O_4[36] and Fe_2O_3.[34]

The CCH single crystals in the composite had the dimensions much the same as in the pristine CCH (Fig. 3c and d). The HRTEM image and the corresponding FFT pattern (Fig. 3e and the inset image) present graphene layers and the CCH atomic planes with a d-spacing of 0.264 nm, corresponding to the (221) reflection.

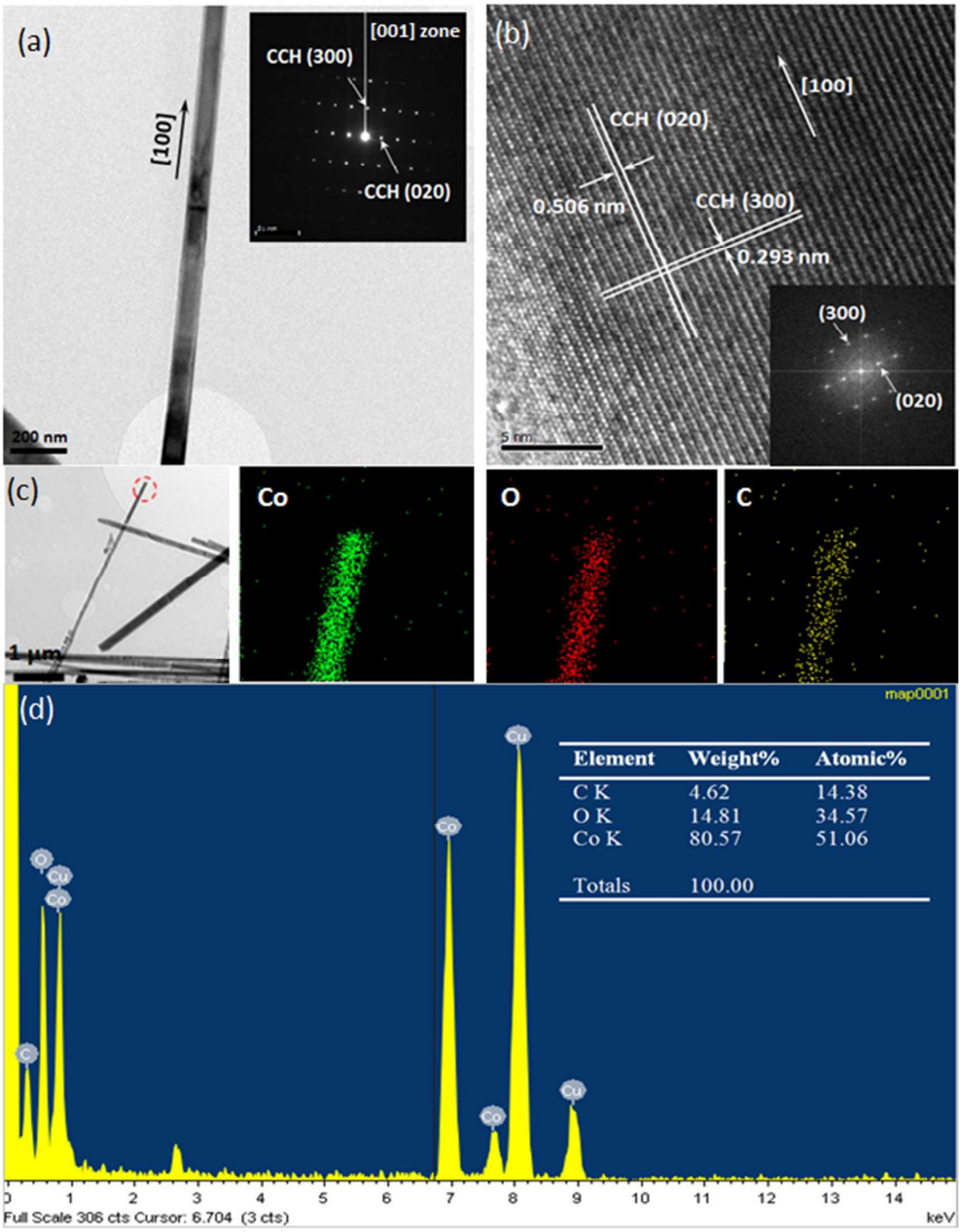

Fig. 2 TEM images of CCH/GA-0 (without graphene): (a) CCH nanowires and SAED pattern in the inset; (b) HRTEM of a CCH single crystal and FFT pattern in the inset; (c) elemental mapping; and (d) EDS analysis.

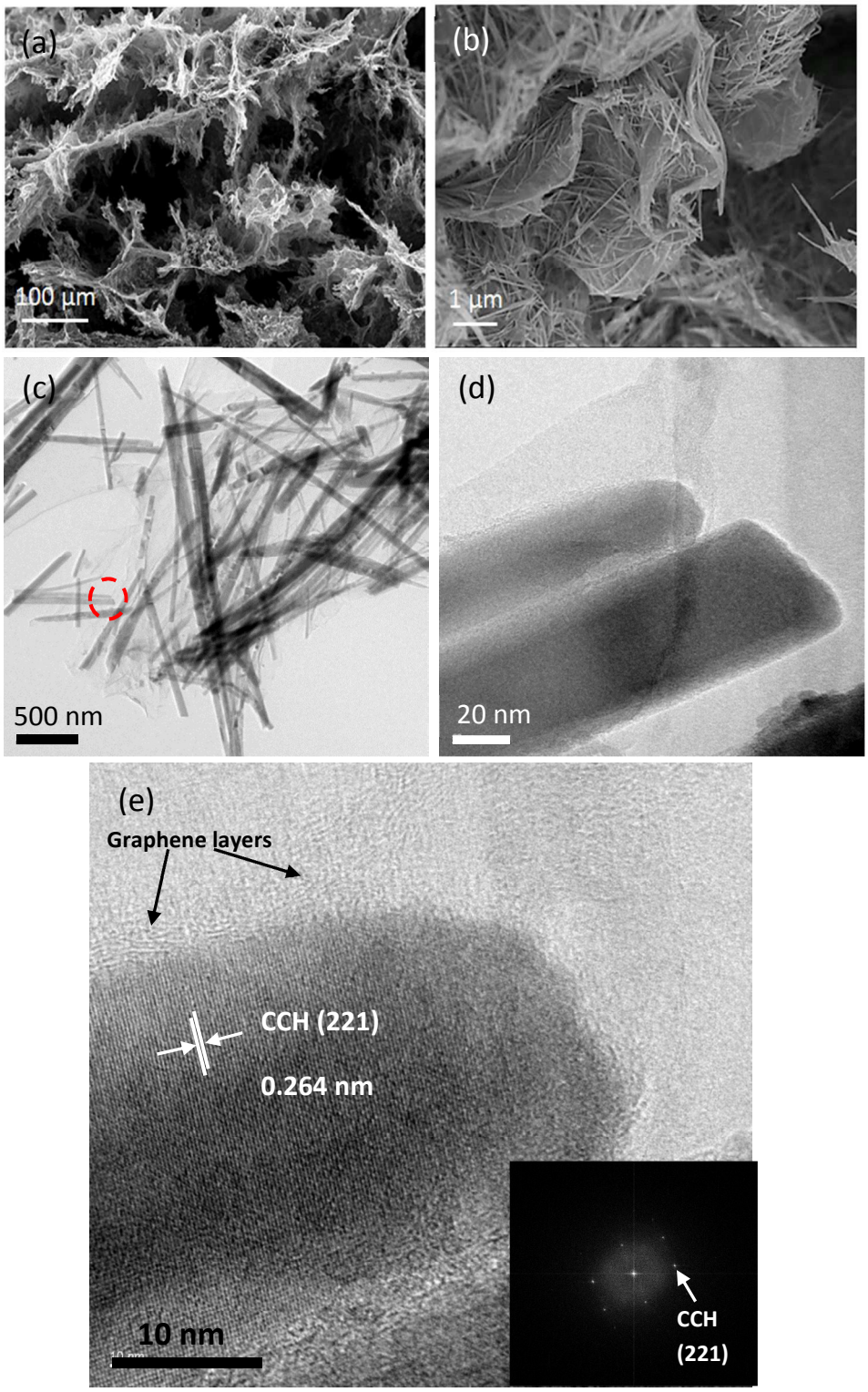

Fig. 3 (a, b) SEM, (c, d) TEM images and (e) HRTEM and FFT pattern of CCH nanowire single crystals on graphene of CCH/GA-2 composite.

The TGA results of all composite samples are shown in Fig. S2. Three distinct steps of weight losses in the CCH/GA composites correspond to (I) the removal of adsorbed water, (II) the dehydroxylation of CCH to cobalt oxide (Co_3O_4) according to Equation 7, and (III) the decomposition of graphene starting from ~350 °C, respectively.[37,38]

$$3Co(CO_3)_{0.5}(OH).0.11H_2O + O_2 \rightarrow Co_3O_4 + 1.5CO_2 + 0.61\ H_2O \quad (7)$$

$$3CoCO_3 + \frac{1}{2}O_2 \rightarrow Co_3O_4 + 3CO_2 \quad (8)$$

However, for the CC/GA composites, the main weight loss appeared at ~370 °C which could be attributed to the decomposition of CC into Co_3O_4 according to Equation 8. In

view of the above oxidation reactions for CCH and CC compounds, the mass loading of Co_3O_4 in the final product, known initial weight of the composites and the molar mass of the compounds participating in the reaction, the mass loadings of CCH or CC in the composites were estimated to be ~62%, 85% and 95% for CCH/GA-1, CCH/GA-2 and CCH/GA-3, respectively, and ~90%, 86% and 88% for CC/GA-1, CC/GA-2 and CC/GA-3, respectively.

The electrochemical performance of the composite electrodes was evaluated at different current densities from 1 to 10 A g^{-1}, and their specific capacitances are summarized in Table 2. The addition of GA into the CCH/GA-0 electrode to form CCH/GA-1 increased the specific capacitance from 316 to 546 F g^{-1} by 230 F g^{-1} at 1 A g^{-1}. The incorporation of 3D-structured GAs with an excellent electrical conductivity of 0.68 S cm^{-1} and a large BET surface area of 167 m^2 g^{-1} into the neat CCH effectively reduced the charge transfer resistance of electrons and offered large redox reaction sites for the electrolyte, giving rise to the capacitance enhancement of the CCH/GA-1 electrode. The increased mass ratio of cobalt precursor to graphene in the CCH/GA-2 electrode led to a surge of capacitance to remarkable 1134 F g^{-1}. However, a further increase in cobalt precursor content adversely affected capacitance due to the reduced electrical conductivity and surface area of the CCH/GA-3 electrode.

Meanwhile, the specific capacitance measured at 1 A g^{-1} decreased with increasing urea content for a given amount of cobalt precursor, from 1134 F g^{-1} for CCH/GA-2 as the optimal CCH electrode, to 478 F g^{-1} for CC/GA-3. Owing to the unfavorable morphology and size of particles, the change in composition significantly reduced the surface area of the active material (Table 1). It is also suspected that the contacts became weaker and the particles tended to be detached from the graphene matrix (Fig. S1), which is partly responsible for the aforementioned capacitance reduction. The CC/GA-1 electrode synthesized with moderate urea content showed the best capacitance performance among all CC/GA electrodes.

Table 2. Specific capacitances of electrodes at different current densities.

Designation	1 A/g	2 A/g	5 A/g	10 A/g
CCH/GA-0	316	292	255	216
CCH/GA-1	546	519	479	400
CCH/GA-2	**1134**	**1004**	**914**	**848**
CCH/GA-3	756	721	624	436
CC/GA-1	**731**	**622**	**567**	**515**
CC/GA-2	626	510	460	426
CC/GA-3	478	459	423	290

Fig. 4 shows the electrochemical performance of the CCH/GA-2 electrode at different scan rates and different current densities. The obvious peaks at specific potentials in the CV curves (Fig. 4a) and the corresponding sloping plateaus in the charge/discharge profiles (Fig. 4b) clearly indicate effective pseudocapacitive properties of the electrode. The gradual change in the shape of the CV curves when the scan rate was increased from 10 to 100 mV s^{-1} suggests excellent electronic conduction within the CCH nanowire/GA composites.[39] Fig. 4c presents the cyclic performance of the CCH/GA-2 electrode in comparison with the neat CCH and CC/GA-1 electrodes measured at a high current density of 10 A g^{-1}. It is worth noting that the specific capacitance of both the composite electrodes, CCH/GA-2 and CC/GA-1, gradually surged in the initial few hundred cycles as a consequence of slow activation of the CC-based electrodes, consistent with the findings in other reports.[40-43] Until the electrolyte fully penetrated into the composite electrode, only a fraction of the active material was activated during the initial few hundred cycles. After the initial stage of cycles, all three electrodes presented very stable capacitances with plateaus between 700 and 1600 cycles, followed by gradual degradation. While they maintained excellent cyclic stability up to 2500 cycles, the overall capacitances were always much higher for the CCH/GA-2 electrode than the other electrodes. There were clear distinctions between the charge/discharge profiles of these electrodes for the first 200 s (Fig. 4d), which further confirmed the beneficial effect of 3D conductive GA as well as the optimized compositions and morphologies of composite electrode materials for enhanced electrochemical performance.[3,19,44]

Fig. 4e compares the rate performance of the three electrodes at different current densities. With increasing current density from 1 to 2, 5 and 10 A g^{-1}, the specific capacitances of CCH/GA-2 gradually reduced from 1134 to 1004, 914 and 848 F g^{-1}, respectively. They are still considerably higher than the corresponding values of the CC/GA-1 and CCH/GA-0 electrodes. Apart from the optimized GA content in the CCH electrodes, i.e. CCH/GA-2 vs CCH/GA-3, the urea content was also an important parameter that determined the rate performance of the electrodes. An excessive urea to cobalt precursor ratio in CC/GA-1 was detrimental to both rate performance and cyclic stability for the aforesaid reasons.

The Nyquist plots obtained from the EIS analysis are shown in Fig. 4f. The EIS data were fitted by Zview software based on an equivalent circuit model (inset of Fig. 4f). The internal resistance, R_s, is the sum of the ionic resistance of electrolyte, the intrinsic resistance of the active material and the contact resistance at the electrode-electrolyte interface; R_{ct} is the interfacial charge-transfer resistance; C_d is the double layer capacitance; and W is the Warburg resistance.[45]The fitted data given in Table S1 show that R_s and R_{ct} of the neat CCH electrode were higher than those of both the CCH/GA-2 and CC/GA-1 electrodes: in particular, R_{ct} of the former electrode was 3-4 times higher than those of the latter two. Besides, the Warburg resistance – the reciprocal of the slope of the EIS curve in the low-frequency range – was lower in the CCH/GA-2 electrode than those of the neat CCH and CC/GA-1 electrodes. These observations confirmed the beneficial effect of graphene on electrochemical characteristics of the composite electrodes.

The optimized sample (CCH/GA-2) was further tested in a symmetric cell and the charge/discharge profiles as well as the CV curves are presented in Figure S3. According to the discharge profiles shown in Figure S3 b and using Equation (1), the device delivered specific capacitances of 122, 86, 46 and 22 F g^{-1} when the current density was changed from 1 to 2, 5 and 10 A g^{-1}. Figure S3c shows excellent capacitance retention by the optimized electrode measured in the CV test at a scan rate of 100 mV s^{-1}. The capacitance retention after 2000 cycles was ~104% compared to the first cycle, indicating excellent cyclic performance of the electrode.

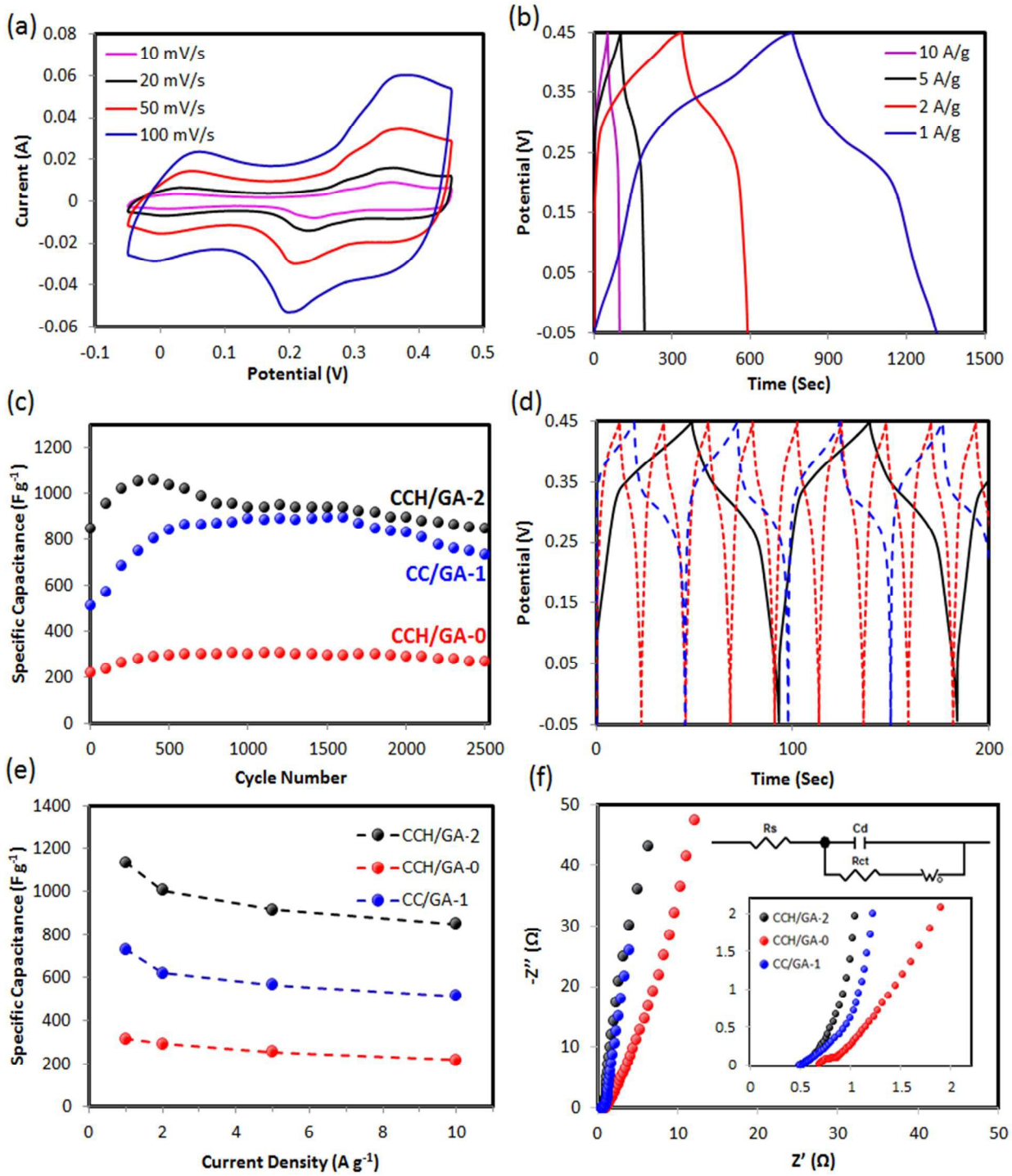

Fig. 4 (a) Typical CV curves at different scan rates and (b) charge/discharge profiles at different current densities of CCH/GA-2 composite electrode; (c) cyclic stability and (d) corresponding charge/discharge profiles measured at 10 A g^{-1}, (e) rate performance at different current densities and (f) EIS spectra measured at open circuit potential of CCH/GA-0, CCH/GA-2 and CC/GA-1 electrodes. The insets of (f) show the enlarged view of Nyquist plots at a high frequency region and the equivalent electrical circuit model.

The above findings signify the potential of carbonate-based materials, both CCH and CC, as active materials in PCs. To the best of our knowledge, however, very limited information is available in the literature about the pseudocapacitive behaviors and reaction mechanisms of CC-based electrodes. Thus, an *ex situ* XPS and CV analyses were conducted in an effort to identify possible pseudocapacitive behaviors of CC compounds. To simplify the analysis and avoid the interference from other materials, neat CC electrodes were prepared on the surface of Ni foam without adding any binders or carbon black, and their electrochemical performance was studied under the same condition. The intrinsic surface redox reactions were specifically looked into by probing the electrode surface after charge and discharge in the first two cycles.

Fig. 5 shows the general and deconvoluted XPS spectra of the CC electrodes in the charge and discharge states. The general spectra (Fig. 5a) were all similar regardless of charge/discharge cycles, except the K 2s peak which appeared at ~ 378 eV after the first charge. The new peak can be attributed to the adsorption of KOH electrolyte on the surface of the electrode material.[44]The O 1s spectra (Fig. 5b) shows a symmetric peak centered at 532.6 eV which belongs to the binding energy of oxygen in the carbonate species of the pristine CC.[47]After the first charging process, two new peaks appeared at 529.7 and 531.4 eV, which correspond to the oxygen bonds in metal oxides and metal hydroxide, respectively.[48,49] In the following discharge process, the peak located at the lower binding energy disappeared while the other two major peaks for metal hydroxide and metal carbonate remained with intensities similar to those of the charge state. Similar changes in binding states of oxygen were observed after the 2nd charge and discharge processes. Fig. 5c exhibits the corresponding Co 2p spectra for the same electrodes. The pristine CC material shows two major peaks at 781.5 and 783 eV for binding energies of Co-hydroxyl and Co-carbonate groups, respectively, along with a satellite feature at 786.3 eV.[32,47,49] After the 1st charge, an extra peak at a low 780.3 eV appeared, an indication of the high oxidation state of cobalt. This peak disappeared upon discharge and reappeared after the 2nd charge process.

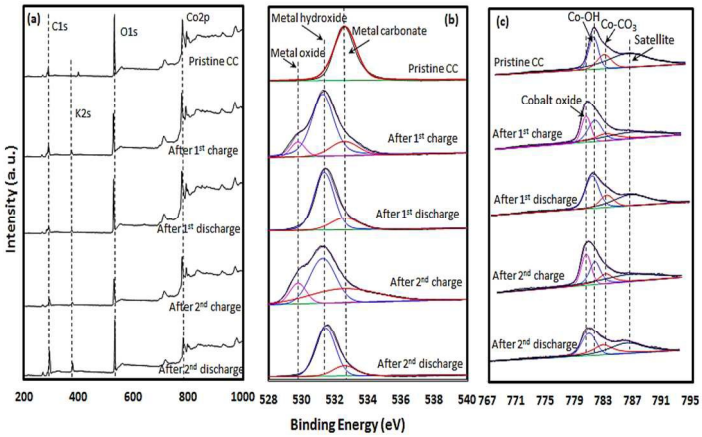

Fig. 5 XPS spectra of pristine CC electrode after the first and second charge and discharge cycles: (a) general spectra; (b) deconvoluted O 1s spectra and (c) deconvoluted Co 2p spectra.

Fig. 6a shows the typical CV curve of CC at a scan rate of 20 mV s^{-1}. Two pairs of redox peaks, (P_1-P_2) and (P_3-P_4), were observed, a typical of pseudocapacitive characteristics. The characteristic symmetry of the anodic and cathodic peaks suggests an excellent electrochemical reversibility for CC as an active material. Based on the aforementioned observations from the XPS analysis and the CV curve, a mechanism is proposed for electrochemical energy storage of CC, which is illustrated in Fig. 6b and summarized as follows. Upon dipping the pristine CC in strong basic KOH electrolyte, the OH units are intercalated into the structure due to the high binding affinity with Co^{+2} cations to form CCH. During the charge process, CCH is oxidized by changing the oxidation state of Co^{+2} first to Co^{+3} and then to Co^{+4}, in good agreement with the peaks, P_1 and P_3, respectively, in the CV curve. Upon discharge, reverse reduction occurs by transforming Co^{+4} to Co^{+3} and then to Co^{+2}, corresponding to the valleys, P_2 and P_4, respectively, in the CV curve. The cobalt-based compounds, such as CC, have long been used as solid intermediates to obtain functional metal oxides using a thermal decomposition process. Cobalt carbonate salts can be easily synthesized via a simple hydrothermal process, thus are a low-cost material. Here, we demonstrate that CC itself has excellent pseudocapacitance properties which can be further improved by incorporating graphene to form nanocomposites as a promising electrode material to replace other types of metal oxides for high performance SCs.

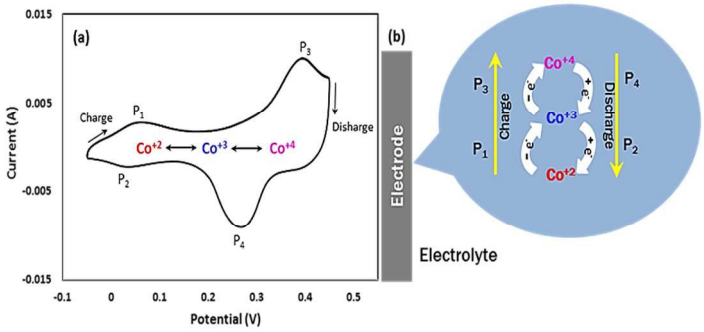

Fig. 6 (a) Typical CV curve of CC-based electrode taken at a scan rate of 20 mV s^{-1} and (b) schematic illustration of redox reactions of cobalt cations on the surface of the electrode in KOH electrolyte.

In summary, the above supercapacitive performance of the CCH/GA-2 and CC/GA-1 electrodes is compared with the electrodes containing metal carbonate compounds reported in the literature, as shown in Table 3. The comparison confirms that the specific capacitances of the current electrodes are among the highest of all electrodes shown for a given current density. The best performing electrode prepared in this study was the cobalt carbonate hydroxide composite (CCH/GA). We also identified the CC/GA composite electrode having excellent pseudocapacitive properties, which has not been reported previously.

Table 3. Comparison of capacitances between different carbonate-based electrodes and the current study.

Materials	Specific Capacitance [F/g]	Current Density [A/g]	Ref.
$MnCO_3$	160	0.5	[15]
$MnCO_3$/graphene hydrogel	645	0.5	[50]
$MnCO_3$	185	1.5	[51]
$MnCO_3$/rGO	368	1.5	[51]
$MnCO_3$/MWCNT	357	1.5	[51]
MnO_2/$MnCO_3$/rGO	194	5 mV s^{-1} (scan rate)	[52]
Nickel hydroxy carbonate	1178	0.5	[53]
Cobalt carbonate hydroxide	1075	5 mA cm^{-2}	[16]
$CoCO_3$/CoO/carbon fiber paper	510	1	[54]
Cobalt carbonate hydroxide/GA	**1134**	**1**	**Current Study**
Cobalt carbonate/GA	**731**	**1**	**Current Study**

4. CONCLUSION

- Cobalt carbonate-based/GA composites, including CCH nanowires and CC microcubes on a GA matrix, were synthesized as high performance SC electrodes via an *in situ* one-pot hydrothermal process without further treatment. Optimal compositions of active material, graphene and urea were identified which produced optimized electrode nano-/micro-structures with balanced supercapacitive performance.
- The addition of GA to form composite electrodes gave rise to much enhanced capacitance. The large surface area of graphene offered large reaction sites that were accessible to electrolyte ions, while its excellent electrical conductivity reduced the charge transfer resistance of electrons, especially for PCs. The inherent 3D nature of GA discouraged agglomeration of active particles during the synthesis process and prevented particles from dropping off during the charge/discharge cycles. These interactions between the active material and GA were responsible for the largely improved capacitive performance of the CCH/GA-2 electrode.
- The optimization of urea content as the source of carbonate and hydroxyl anion groups during the hydrothermal process allowed one to not only control the composition and nano-/micro-structure of the composite, but also the resultant pseudocapacitive performance of the CCH- and CC-based electrodes.
- A pseudocapacitive mechanism of CC compounds is proposed through the *ex situ* XPS analysis of the electrodes after charge and discharge processes. The reversible redox reactions of cobalt cations are found to be responsible for pseudocapacitive properties. The characteristic symmetry of the anodic and cathodic peaks revealed from the CV curves suggests an excellent electrochemical reversibility of the CC electrodes. These findings can shed insights into developing similar transition metal compounds as potential active materials for high performance SCs.

Acknowledgements

This project was financially supported by the Research Grants Council (GRF Project codes: 613612 and 16212814) and the Innovation and Technology Commission (ITF Project code: ITS/318/14) of Hong Kong SAR. The authors also appreciate the technical assistance from the Materials Characterization and Preparation Facilities (MCPF) and the Department of Chemical and Biomolecular Engineering at HKUST.

Notes and references

[a] Department of Mechanical and Aerospace Engineering, The Hong Kong University of Science and Technology, Clear Water Bay, Hong Kong
*Email: mejkkim@ust.hk

Electronic Supplementary Information (ESI) available: [SEM images of CC/GA-1 and CC/GA-3, TGA analysis, EIS results and electrochemical performance of two-electrode configuration]. See DOI: 10.1039/b000000x/

1 P. Simon, Y. Gogotsi, *Nat. Mater.* 2008, **7**, 845.
2 X. Lu, M. Yu, G. Wang, Y. Tong, Y. Li, *Energy Environ. Sci.* 2014, **7**, 2160.
3 H. Jiang, P. S. Leeb, C. Li, *Energy Environ. Sci.* 2013, **6**, 41.
4 L. L. Zhang, X. S. Zhao, *Chem. Soc. Rev.* 2009, **38**, 2520.
5 R. Raccichini, A. Varzi, S. Passerini, B. Scrosati, *Nat. Mater.* 2015, **14**, 271.
6 M. D. Stoller, S. Park, Y. Zhu, J. An, R. S. Ruoff, *Nano Lett.* 2008, **8**, 3498.
7 V. Augustyn, P. Simon, B. Dunn, *Energy Environ. Sci.* 2014, **7**, 1597.
8 G. Wang, L. Zhang, J. Zhang, *Chem. Soc. Rev.* 2012, **41**, 797.
9 G. Zhang, X. W. D. Lou, *Adv. Mater.* 2013, **25**, 976.
10 P. Yang, Y. Ding, Z. Lin, Z. Chen, Y. Li, P. Qiang, M. Ebrahimi, W. Mai, C. P. Wong, Z. L. Wang, *Nano Lett.* 2014, **14**, 731.
11 J. Tang, D. Liu, Y. Zheng, X. Li, X. Wang, D. He, *J. Mater. Chem. A* 2014, **2**, 2585.
12 Y. Tang, Y. Liu, S. Yu, S. Mu, S. Xiao, Y. Zhao, F. Gao, *J. Power Sources* 2014, **256**, 160.
13 X. Sun, G. Wang, H. Sun, F. Lu, M. Yu, J. Lian, *J. Power Sources* 2013, **238**, 150.
14 H. Li, X. Duan, J. Ma, W. Zheng, *Cryst. Res. Technol.* 2012, **47**, 25.
15 S. Devaraj, H. Y. Liu, P. Balaya, *J. Mater. Chem. A* 2014, **2**, 4276.
16 Z. Lu, W. Zhu, X. Lei, G. R. Williams, D. OHare, Z. Chang, X. Sun, X. Duan, *Nanoscale* 2012, **4**, 3640.
17 X. Peng, L. Peng, C. Wu, Y. Xie, *Chem. Soc. Rev.* 2014, **43**, 3303.
18 C. Xiang, M. Li, M. Zhi, A. Manivannan, N. Wu, *J. Power Sources* 2013, **226**, 65.
19 M. Zhi, C. Xiang, J. Li, M. Li, N. Wu, *Nanoscale* 2013, **5**, 72.
20 L. Li, Z. A. Hu, N. An, Y. Y. Yang, Z. M. Li, H. Y. Wu, *J. Phys. Chem. C* 2014, **118**, 22865.
21 G. H. An, H. J. Ahn, *Carbon* 2013, **65**, 87.
22 F. Zhou, Q. Liu, J. Gu, W. Zhang, D. Zhang, *J. Power Sources* 2015, **273**, 945.
23 Z. D. Huang, B. Zhang, Q. Zheng, S. W. Oh, X. Y. Lin, N. Yousefi, J. K. Kim, *J. Mater. Chem.* 2012, **22**, 3591.
24 Y. B. Tan, J. M. Lee, *J. Mater. Chem. A* 2013, **1**, 14814.
25 J. Zhu, Y. K. Sharma, Z. Zeng, X. Zhang, M. Srinivasan, S. Mhaisalkar, H. Zhang, H. H. Hng, Q. Yan, *J. Phys. Chem. C* 2011, **115**, 8400.
26 D. Wang, Q. Wang, T. Wang, *Inorg. Chem.* 2011, **50**, 6482.
27 S. Xiong, J. S. Chen,X. W. Lou,H. C. Zeng, *Adv. Funct. Mater.* 2012, **22**, 861.
28 Y. Geng, S. J. Wang, J. K. Kim, *J. Colloid Interf. Sci.* 2009, **336**, 592.
29 Q. Zheng, W. H. Ip, X. Lin, N. Yousefi, K. K. Yeung, Z. Li, J. K. Kim, *ACS Nano* 2011, **5**, 6039.
30 T. Y. Kim, G. Jung, S. Yoo, K. S. Suh, R. S. Ruoff, *ACS Nano* 2013, **7**, 6899.
31 S. Abouali, M. Akbari Garakani, B. Zhang, Z. L. Xu, E. Kamali Heidari, J. Huang, J. Q. Huang and J. K. Kim, *ACS Appl. Mater. Interfaces* 2015, **7**, 13503.
32 M. Akbari Garakani, S. Abouali, B. Zhang, C. A. Takagi, Z. L. Xu, J. Q. Huang, J. Huang, J. K. Kim, *ACS Appl. Mater. Interfaces* 2014, **6**, 18971.
33 C. C. Li, X. M. Yin, T. H. Wang, H. C. Zeng, *Chem. Mater.* 2009, **21**, 4984–4992.
34 T. Yang, Z. Huang, Y. Liu, M. Fang, X. Ouyang, M. Hu, *Ceram. Int.* 2014, **40**, 11975.
35 G. Cheng, Y. Yan, R. Chen, *New J. Chem.* 2015, **39**, 676.
36 H. Du, L. Jiao, Q. Wang, Q. Huan, L. Guo, Y. Si, Y. Wang, H. Yuan, *CrystEngComm* 2013, **15**, 6101.
37 Z. Zhao, F. Geng, J. Bai, H. M. Cheng, *J. Phys. Chem. C* 2007, **111**, 3848.
38 X. Xie, P. Shang, Z. Liu, Y. Lv, Y. Li, W. Shen, *J. Phys. Chem. C* 2010, **114**, 2116.
39 H. B. Li, M. H. Yu, X. H. Lu, P. Liang, J. Xiao, Y. X. Tong, G. W. Yang, *ACS Appl. Mater. Interfaces* 2014, **6**, 745.
40 X. Xia, J. Tu, Y. Zhang, Y. Mai, X. Wang, C. Gu, X. Zhao, *RSC Adv.* 2012, **2**, 1835.
41 X. C. Dong, H. Xu, X. W. Wang, Y. X. Huang, M. B. C. Park, H. Zhang, L. H. Wang, W. Huang, P. Chen, *ACS Nano* 2012, **6**, 3206.
42 X. Xiong, D. Ding, D. Chen, G. Waller, Y. Bu, Z. Wang, M. Liu, *Nano Energy,* 2015, **11**, 154.
43 S. Abouali, M. Akbari Garakani, B. Zhang, H. Luo, Z. L. Xu, J. Q. Huang, J. Huang, J. K. Kim, *J. Mater. Chem. A* 2014, **2**, 16939.

44 Q. Guan, J. Cheng, B. Wang, We. Ni, G. Gu, X. Li, L. Huang, G. Yang, F. Nie, *ACS Appl. Mater. Interfaces* 2014, **6**, 7626.
45 K. Qiu, Y. Lu, D. Zhang, J. Cheng, H. Yan, J. Xu, X. M. Liu, J. K. Kim and Y. S. Luo, *Nano Energy* 2015, **11**, 687.
46 K. Chen, S. Song, K. Li, D. Xue, *CrystEngComm* 2013, **15**, 10367.
47 J. Yang, H. Cheng, R. L. Frost, *Spectrochim. Acta A,* 2011, **78**, 420.
48 J. K. Chang, M. T. Lee, C. H. Huang, W. T. Tsai, *Mater. Chem. Phys.* 2008, **108**, 124.
49 J. K. Chang, C. M. Wu, I. W. Sun, *J. Mater. Chem.* 2010, **20**, 3729.
50 J. Yuan, J. Zhu, H. Bi, Z. Zhang, S. Chen, S. Liang, X. Wang, *RSC Adv.* 2013, **3**, 4400.
51 D. Ghosh, S. Giri, S. Dhibar, C. K. Das, *Electrochim. Acta* 2014, **147**, 557.
52 Y Liu, D He, H Wu, J Duan, Y Zhang, *Electrochim. Acta* 2015, **164**, 154.
53 G. Zhu, C. Xi, M. Shen, C. Bao, J. Zhu, *ACS Appl. Mater. Interfaces* 2014, **6**, 17208.
54 X. Ji, S. Cheng, L. Yang, Y. Jiang, Z. Jiang, C. Yang, H. Zhang, M. Liu, *Nano Energy* 2015, **11**, 736.

